View metadata, citation and similar papers at core.ac.uk
brought to you by CORE
provided by Brunel University Research Archive

Modelling and empirical development of an anti/de-icing approach for wind turbine blades through superposition of different types of vibration

Hossein Habibi[*1], Graham Edwards[†], Caumaghen Sannassy[*], Vassilios Kappatos[*], Yoann Lage[†], Jasmin Stein[†], Cem Selcuk[*], Tat-Hean Gan[*,†]

[*] Brunel Innovation Centre (BIC), Brunel University London, Uxbridge, Middlesex, UB8 3PH, United Kingdom
[†] TWI Ltd, Granta Park, Great Abington, Cambridge, CB21 6AL, United Kingdom

Abstract

The generation of green, safe and inexpensive energy by wind turbines is often decreased or interrupted in severe climate areas during cold weather. When the blades are even partially covered by different types of ice their efficiency drops suddenly due to degradation of the blade profile from the ideal. The present study presents a new approach using ultrasonic guided waves as an anti/de-icing technique supplemented by low frequency vibrations to effect shedding of the ice from the turbine blades. The study consists of a series of steps including initial theoretical studies and finite element simulation of representative plates and turbine blades, followed by a number of experimental validations concluded by tests of the complete approach in an icing wind tunnel. The results show the efficacy of the developed approach in tackling the different types of ice which can form on the blades, using very low power compared to available thermal techniques.

Keywords: wind turbine blades, anti-icing, de-icing, vibration, ultrasonic guided waves

1. Introduction

Today, wind energy is an efficient source to supply green power. The relatively cheap and reliable harvest of this energy has extended its use into wide geographical regions, even those with an icing climate. However the power generation by wind turbines in such regions usually suffers from the harshness of the weather in mid-winter when the wind turbine blades are subject to ice formation. It has been well reported that ice accretion on wind turbine blades can drop the turbine efficiency and reduce output power [1, 2, and 3]. To solve the icing problem, a range of techniques has been developed and applied to date. Thermal technologies including electrical resistance heating and hot air circulation have shown some success but they are usually energy inefficient as they consume considerable amounts of energy themselves. For example, hot air circulation can use up to 15% of the turbine's nominal output power [2]. Some attempted/proposed methods such as microwave heating have poor performance [3]. Likewise, other available techniques including coating and

[1] Corresponding author; emails: Hossein.Habibi@brunel.ac.uk, bic@brunel.ac.uk, Tel: +44(0)1223 899000

painting blades, use of anti-freeze chemicals and active pitching are associated with major drawbacks such as excessive heat absorption, damage risk to structural integrity of the blades, and environmental pollution [4].

In this work, an approach has been proposed and tested to overcome the icing problem effectively for the blades of a 75-kW wind turbine using relatively little energy. The technique exploits the advantages of two previously attempted techniques in a synergistic way to cover up one another deficiencies. These two techniques are Ultrasonic Guided Waves (UGW) and Low Frequency Vibrations (LFV). The main action is carried out by application of UGW which has been used for non-destructive testing for many decades but it is relatively new as an ice protection technique. Guided waves are considered as the long-range waves propagating through materials in which vibrations of high frequency compared to LFV are created on the surfaces. The technique of UGW has recently been considered to be developed, improved or adapted in different ways for protecting surfaces against icing [5, 6, 7]. The idea in this approach is to induce shear stress at the interface of ice with blade outer surface sufficient to de-bond the accreted ice layer. The challenge is how to excite the appropriate waves that generate such an effective stress on the material surfaces. This depends on factors such as wave mode, excitation frequency, direction of excitation, and the arrangement of a possible transducer array, and requires that the dispersion curves of the propagating waves be extracted and analysed. The analysis can be very complicated due to the complex geometry of the blade. Moreover, it is very important to select an optimum frequency and wave mode at which minimum power is consumed consistent with the required shear stress at the ice layer/blade substrate being produced. For this reason, a so-called interfacial stress concentration coefficients (ISCC) factor has been developed previously to characterise the wave mode, minimal power and frequency maximising the shear stress induced at the interface (see [8] for details). The ISCC values should be then superimposed with dispersion curves to complete the criteria for selection of excitation frequency. According to the definition of ISCC, the higher ISCC, the more shear stress can be induced at the ice interface. So a frequency band with high ISCC value is the first criterion. Dispersion is normally defined as the dependency of the wave velocity on the frequency at which wave propagates in a medium. One of the desirable characteristics for an ideal wave mode in UGW applications is having lower dispersion i.e. the less variation of wave properties with frequency. In addition, it is very important to avoid energy dispersion and dissipation by selecting a non-dispersive frequency range for the wave mode. Moreover, it should be noted that dispersive wave modes undergo more attenuation and therefore less coverage than non-dispersive ones. So the second criterion to be taken into account is selection of a wave mode without any or with minimum dispersion.

The complementary action in this approach is provided by LFV which was first utilised by Bell Helicopter to tackle ice formation on helicopter blades [9]. It showed successful results on the blades except in the vicinity of the leading edges. In the current work, LFV plays a supplementary role to ensure that the ice will be shed simultaneously with or immediately after the ice/substrate bond is weakened by UGW action. The idea is based on generation of high accelerations, from 25g to 30g, enough to cause stress at the blade surface. These levels of acceleration and stress can be reached at a frequency close to one of the first 4-6 natural

frequencies of the blade between 0 and 50 Hz. It should also be stated that the wave frequency must not match the resonance frequency precisely due to possible risk of damage to structural integrity of the blade. Accordingly this level of vibration should not be applied for more than two seconds to prevent reduction in fatigue life according to the original studies in this area [9].

In the following section, a summary of the computer simulation and numerical modelling will be presented. Then some of the prominent results from laboratory trials that validate the model findings are illustrated. Finally the experimental setup and outcome of this new approach in an icing climatic chamber will be demonstrated.

2. N**umerical modelling**

As mentioned above, the proposed strategy combines two types of vibration burdening technique at both low frequency (below 50 Hz) and high frequency (10 - 20 KHz). Each technique however needs to be first individually configured and optimised according to its own criteria and requirements in order to be suitable for superposition in the final synergistic approach.

2.1. Ultrasonic guided waves

Regarding the UGW, the first step is to work out the dispersion curves superimposed with ISCC values for determining the most appropriate wave mode and frequency. This procedure was initiated with modelling of the leading edge of the blades using different thicknesses as well as with different thickness for ice. The ice properties were selected according to a specific type called glaze ice which is one of the most common types forming on wind turbine blades. For example, Fig. 1 represents the combination of dispersions with ISCC values for a 7-mm thick composite blade covered with a 2-mm glaze ice layer. The brightest dots encircled by yellow ellipses indicate the area of highest ISCC. Although it is not quite clear exactly which wave mode should be picked due to the complication of the composite blade geometry, the clustering of several points with high ISCC values implies the central frequency for excitation signal. According to this diagram, the central frequency of the excitation signal should be f=14.86 kHz which corresponds to a phase velocity of v=2093.5 m/s. Since $v = f\,\lambda$, the wavelength would be $\lambda = 0.1409$ m which is the value considered in calculating the best distance between the transducers. A trial process was then applied on a representative plate with different thickness for a modelled ice layer to figure out the best possible scenario for a transducer array. A sample of these simulations can be seen in Fig. 2 which shows the distribution of *von Mises* stress over the plate caused by the propagating waves using a 4-by-4 array and trying different sets of transducer distance in vertical and horizontal directions. In conclusion, a pair of transducers placed $\lambda/4$ away in a vertical direction leads to the best stress distribution and energy concentration on a target line, e.g. the leading edge.

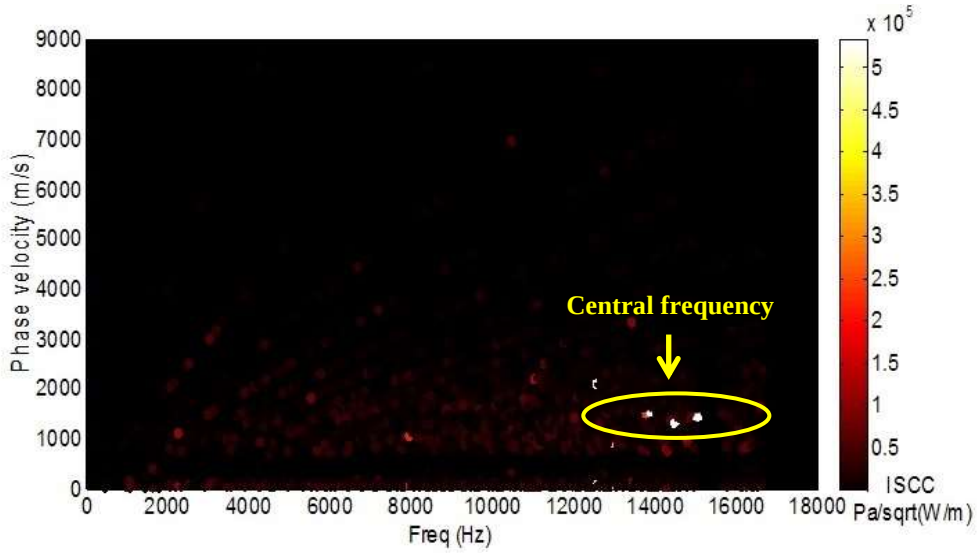

Fig. 1: Dispersion of a 7-mm thick blade's leading edge with a 2-mm thick layer of glaze ice superimposed with ISCC values

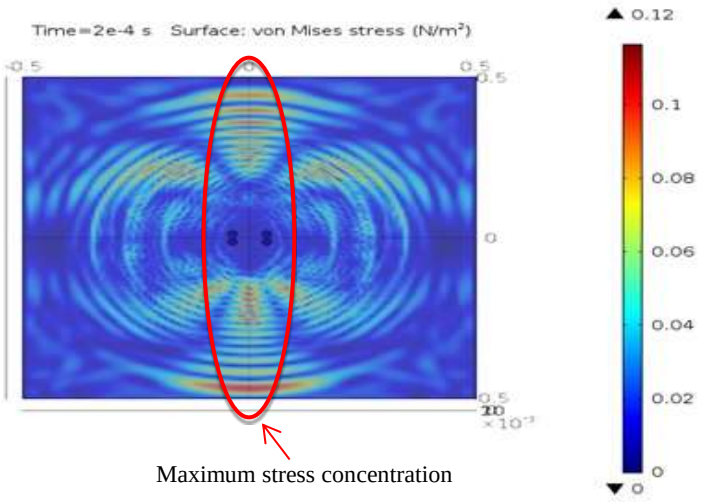

Fig. 2: Aluminium plate with 2mm-thick glaze ice at 150 μs

In addition to the modelling trials for configuring the transducer array, the best excitation direction of the transducers was also investigated. Based on all the scenarios modelled and analysed, it was inferred that a pair of transducers placed at the centre of a 1m-long section of a representative blade leading edge excited in the direction *Z* (see Fig. 3) leads to the most efficient result which is the propagation of wave as uniformly as possible on the blade surface to create required level of stress in the most of the area. Figure 3 shows the wave propagation and the resulting distribution of *von Mises* stress at two different times. The input was applied as a force per unit area (selected to be 1 MN/m^2 in this case as an optimum value) on the transducers. As seen in these two diagrams, although the wave does propagate into the composite blade materials, the level of stress caused in the blade surface is not high enough for de-bonding the ice layer due to attenuation. According to previous experimental studies, a range of stress from 0.5 to 3 MPa is required for de-icing [10, 11]. In fact the composite blade

section was subject to a rapid attenuation as the waves travel along the blade away from the transducers. One solution to this problem is using more transducers to cover broader surfaces. However, it would lead to more energy consumed which degrades the efficiency advantage of the technique. For this reason, a different approach as attachment of an aluminium shield on the leading edge was proposed and studied as will be explained in the next section. This shield not only improves the effectiveness of the wave propagation which leads to higher shear stress while consuming lower power, but it can also serve for other purposes, e.g. protection against lightning strike. The properties corresponding to the composite blade model and the aluminium shield used for the leading edge are given in Table 1.

Table 1: Mechanical properties of composite blade and aluminium shield

Mechanical properties	Density (kg/m^3)	E_1 (GPa)	E_2 (GPa)	E_3 (GPa)	G_{12} (GPa)	G_{13} (GPa)	G_{23} (GPa)	ν_{23}	ν_{12}	ν_{13}
Fibreglass composite used for the blade model	1860	5.62	4.59	4.59	0.41	0.41	0.28	0.24	0.22	0.22
Aluminium used for the shield	2700	70.3			--			0.345		

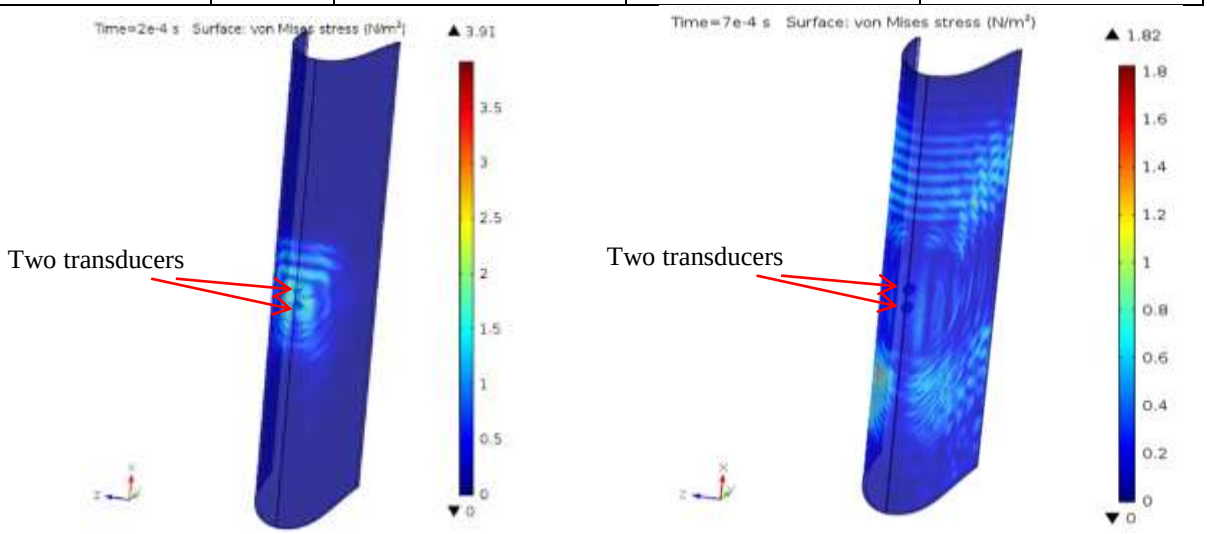

Fig. 3: Wave propagation in a representative section for blade leading edge at *a*) t=2e-4 sec; b) t=7e-4 sec.

2.2. Low frequency vibrations

In terms of LFV, the modelling process consists of two main parts, i.e. modal analysis and harmonic analysis through which the best points to induce vibrations are characterised. Figure 4 shows the first four mode shapes of the blade derived via the finite element software COMSOL Multiphysics. The blade modelled in COMSOL is 4.5 m long in which a standard internal structure including skin, spar (shear webs) and caps are considered. This three-

dimensional FEM model was constructed using element SHELL181 which is usually an appropriate choice for modelling composite shells and lay-up plates. The blade was generated by 17354 shell elements in total with an increased mesh density towards the edges. Fixed boundary conditions in all directions and rotations were then applied to the root of the blade.

The first three modes are flexural bending modes in either flapwise or edgewise directions and the fourth mode is torsional. This analysis was carried out to determine the places that can generate the required acceleration (i.e. 25g -30g, [9]) which leads to sufficient shear stress at the blade surface for de-icing action. For this reason, it is important to excite the proper modes through shakers mounted at the correct points, i.e. the antinodes corresponding to those modes. Having studied all the low frequency modes, the three points indicated in Fig. 5 were chosen as the best potential places to be used for a shaker set-up. This arrangement was capable of generating enough acceleration in such a way that the created stress does not exceed the threshold for reduction in fatigue life of the blade (below 10^6 - 10^7 cycles, [12]). This setup is aimed to excite the third mode shape at a frequency close to its natural frequency, i.e. 25.91 Hz. (Note that the operational frequency should not precisely match the natural frequency but only be picked in its vicinity.) For this reason, harmonic analysis of the blade was carried out to monitor the frequency-domain response of the model from 0 to 50 Hz. Figure 6 depicts this response as displacement versus frequency in which the resonance frequency corresponding to the third mode shape (f=25.91 Hz) is of high interest as it can cause required stress on the blade while not exceeding stress which poses damage to the blade in terms of reduction in fatigue life. In Fig. 7, the stress distribution in the ice layer modelled on the blade, due to application of the optimal shaker set-up at f= 26.2 Hz is displayed. As can be seen, the created stress in this mode is high enough to remove the ice while the maximum stress generated due to the first and second mode shapes was sufficient to cause considerable fatigue life reduction to the blade.

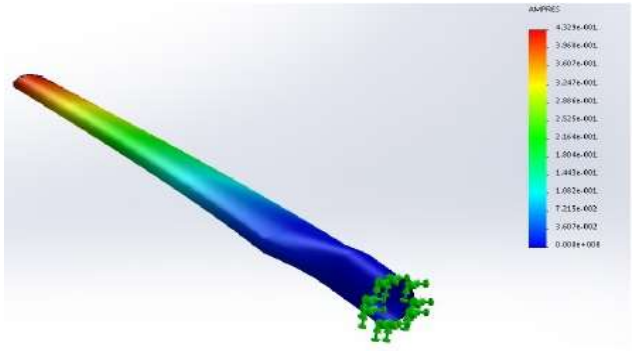

1st mode shape: first flexural bending in flapwise; f=5.58Hz

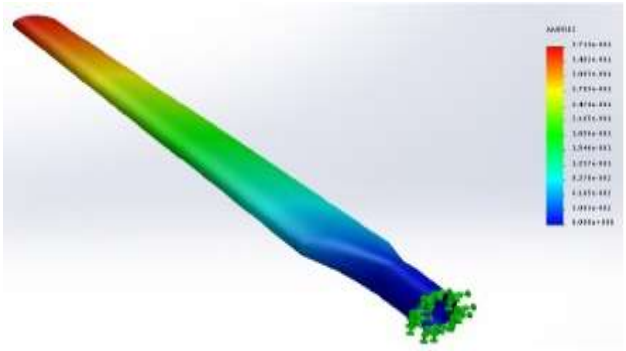

2nd mode shape: flexural bending in edgewise; f= 10.72 Hz

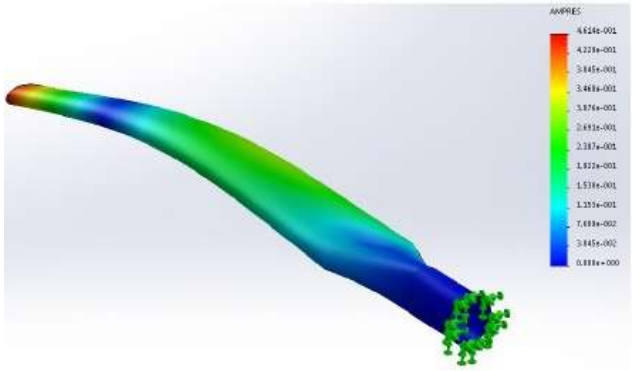

3rd mode shape: second flexural bending in flapwise; f= 25.91 Hz

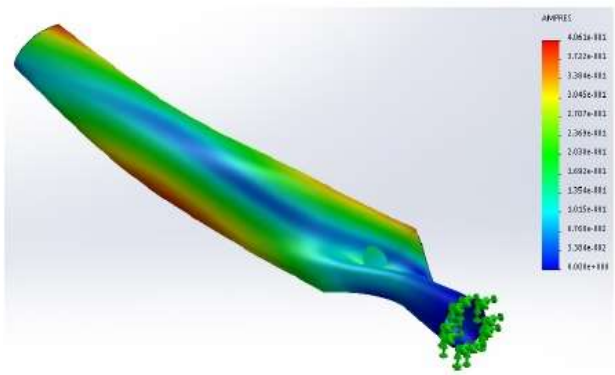

4th mode shape: first torsional mode; f= 49.17 Hz

Fig. 4: The first four mode shapes of the developed blade model

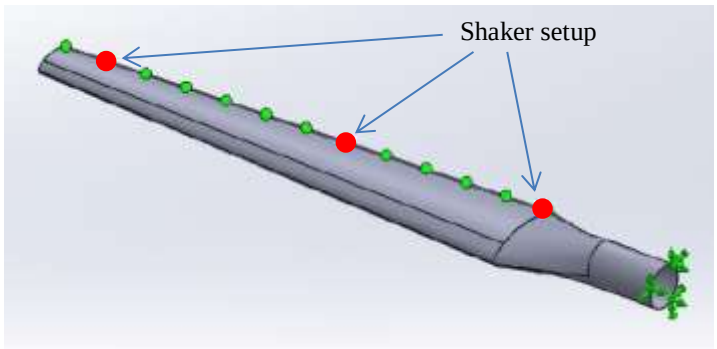

Fig. 5: An optimal shaker setup to induce LFV on the blade model

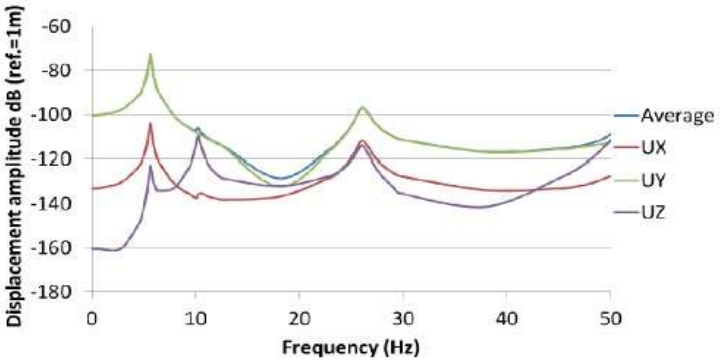

Fig. 6: Displacement frequency-response of the blade model between 0 to 50 Hz in three spatial directions (Ux, Uy and Uz)

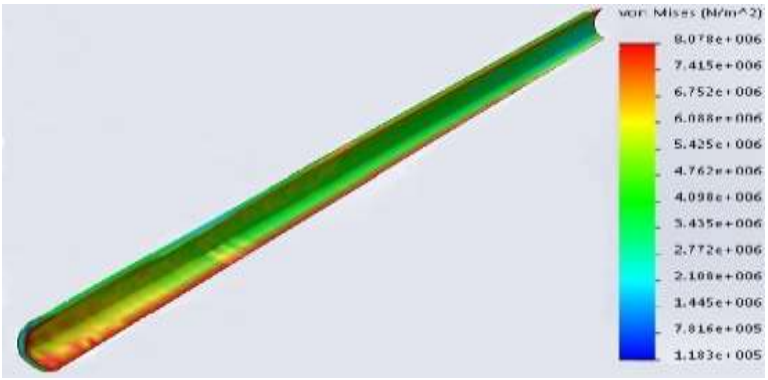

Fig. 7: Stress distribution in the modelled ice layer

3. Experimental validation

3.1. Laboratory trials

In order to predict the capability of the developed approach for tackling ice formation on the wind turbine blade, a number of laboratory tests were carried out prior to the wind tunnel trials through using a low-cost thermal chamber and basic standard equipment. The tests were implemented for both techniques, UGW and LFV, separately using different samples as each technique demands its own criteria and conditions for optimum performance.

3.1.1. LFV tests

There are a few parameters through which the empirical data can yield to demonstrate and validate the modelling results to ensure that the selected operational values meet the de/anti-icing criteria while no ice is used for the LFV experiments described as follows.

3.1.1.1 Strain gauge setup

One of these parameters is the operational frequency of the shaker whose effectiveness can be verified through checking appropriate strain/displacement induced on the blade. As one method, five strain gauges were installed along the blade longitudinal axis, as shown in Fig. 8, to measure the displacement of five different points of the blade while the harmonic force frequency was swept up to 30 Hz. Shown is also Fig. 9 in which the dimensions of the blade and the coordinates of the five strain guages are specified. This setup should reveal the suitability of the operational frequencies determined by the modelling results. For this reason, the readings by the sensors undergoing strain needed to be processed. According to the measurements, the third mode shape which has the natural frequency at 26.2 Hz vibrating the blade in the flapwise direction is highly effective due to the maximum amount of required strain generated on the blade surface at this mode/frequency.

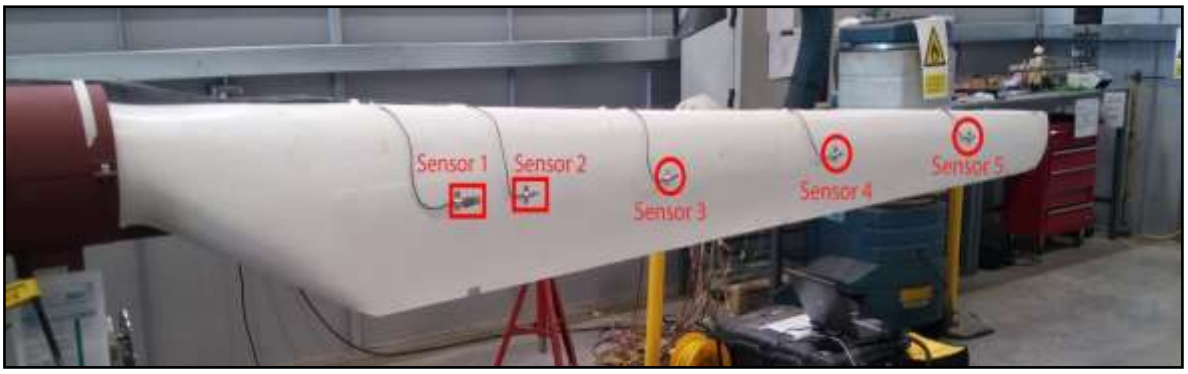

Fig. 8: Experimental strain gauge setup indicating position and number of the sensors (strain gauges) on the blade

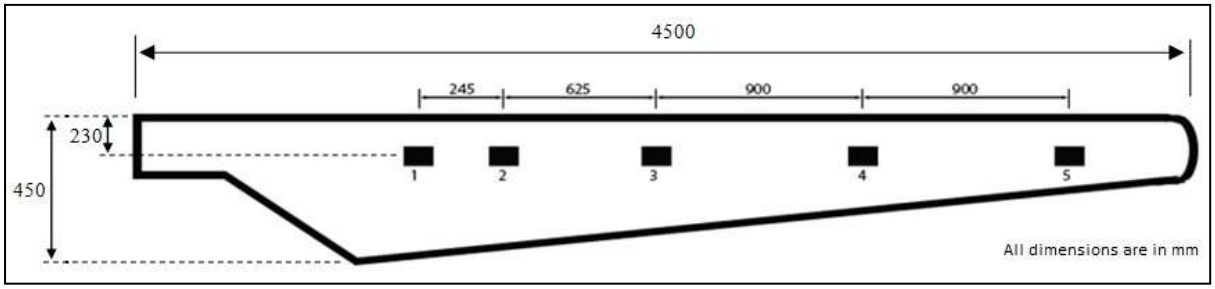

Fig. 9: Dimensions of the blade and positions of the five installed strain guages

As a first example, Fig. 10 shows the shear strain recorded by sensor 2 over the first 0.25 seconds at four frequencies. More frequencies could have been displayed here but to avoid confusion in the diagram, only a few frequencies around f=25 Hz have been presented.

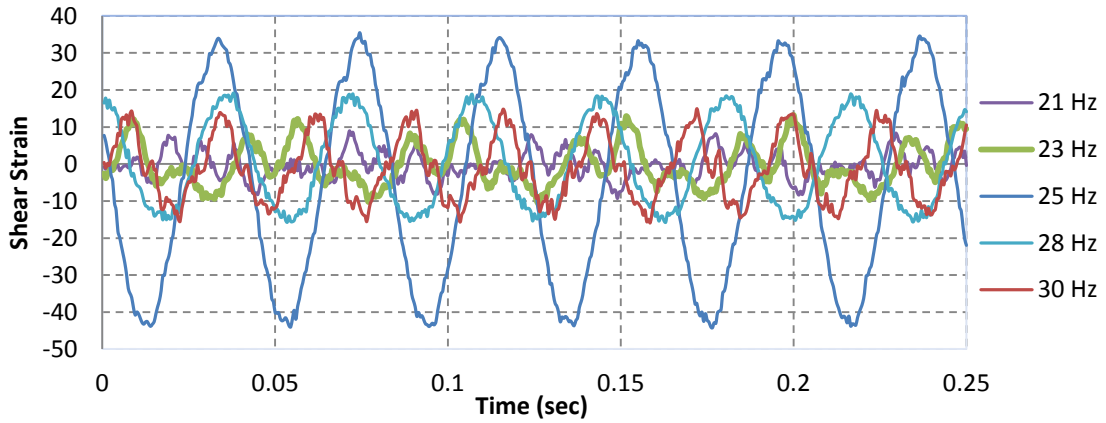

Fig.10: Variations of shear strain recorded by sensor 2 over time at a few frequencies around f=25 Hz

As can be seen in Fig. 10, sensor 2 records the highest values of shear strain at 25 Hz which is consistent with the modelling results. Likewise, the data taken from other sensors confirm the same trend as sensor 2.

Finally, to have an overall view of the performance of all low frequencies tested on the blade over the full-time operational period from 0 to 10 seconds, Fig. 11 displays the

maximum shear strain recorded by all 5 sensors. As can be seen, for the first two sensors taking the data from the critical points of the blade, i.e. close to the hub, the maximum shear strain by far occurs for the third mode shape. For the other three sensors, although the shear strain does not maximise at f=25 Hz, there is still a high amount of strain at this frequency- noting that the last three points are not as crucial as the first two ones in terms of being prone to ice accretion. For this reason, the frequency at which the first sensors show higher values should be considered top priority. Thus, f=25 Hz should be selected as the optimum operational frequency for the induced low-frequency vibration of the blade.

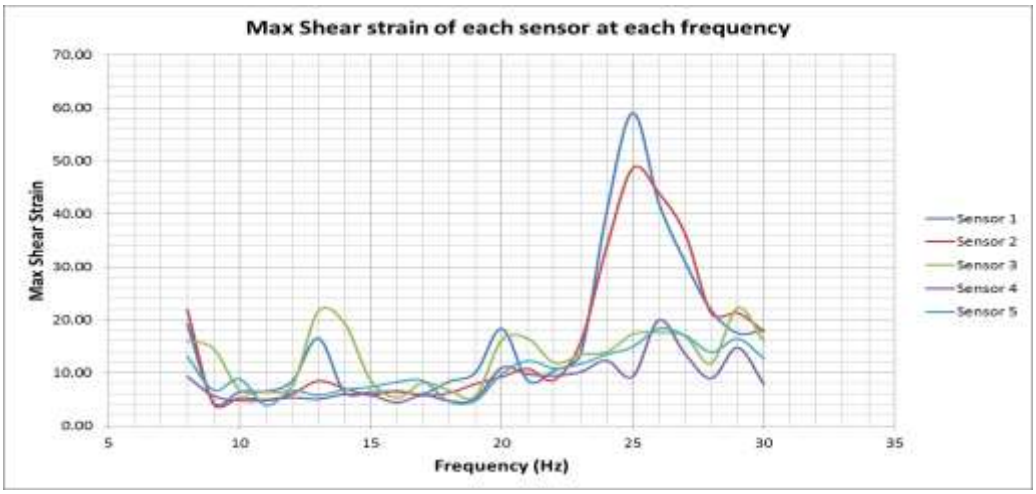

Fig. 11: Representation of maximum shear strain recorded by the 5 strain gauges mounted on the blade over a 10-sec operational period versus a frequency spectra from 8 Hz to 30 Hz.

3.1.1.2 Operational modal analysis

Another verification of the modelling results is via operational modal analysis to work out the mode shapes of the blade and hence the optimal excitation frequency. The experimental setup adopted for this experiment is shown in Fig.12 where the shaker (eccentric rotating mass) has been fitted inside the root of the blade generating the harmonic force.

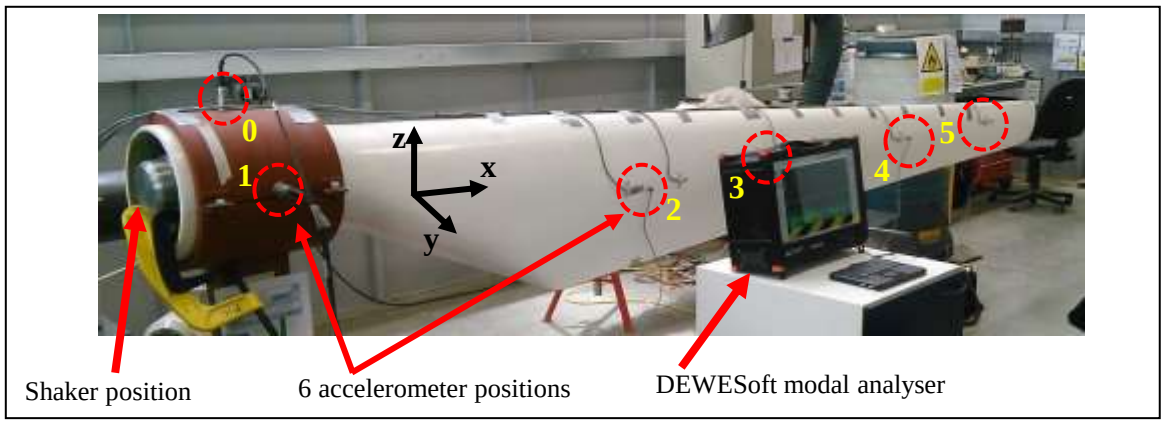

Fig. 12: Experimental setup for modal analysis using 6 piezoelectric accelerometers.

The acceleration responses are measured in six different positions; five along the longitudinal axis of the blade (root to tip) to measure acceleration in the horizontal direction (y) and one, numbered 0, in the root of the blade to measure vertical acceleration (z). The

coordinates of these six accelerometers are displayed in Table 2. Fourier analysis was performed by a commercial system, DEWESoft's SIRIUS R8. Measurements were performed over 10 seconds with 20 kHz sampling rate at each excitation frequency between 0 and 35 Hz. Each excitation frequency is adjusted manually and the software rerun in each case. Then the Fourier spectrum of acceleration is calculated by the software, making it possible to visualise data during the experiment and record it in a *txt* file for post-processing.

Table 2: Accelerometer positions on the blade

Accelerometer No.	Distance from blade root (mm)	Measurement direction
0	200	z
1	200	y
2	1400	y
3	2240	y
4	3140	y
5	4040	y

Using the commercial software MatLab, a routine was created to extract and plot the data (amplitude spectrum values of accelerations) from all the *txt* files. These results were recorded as 3D plots and represent the acceleration response spectrum for each individual accelerometer reading as a function of the frequency response of the structure and the excitation frequency. As an instance, the plot in Fig. 13 shows the spectrum for accelerations taken at accelerometer 2, close to the hub.

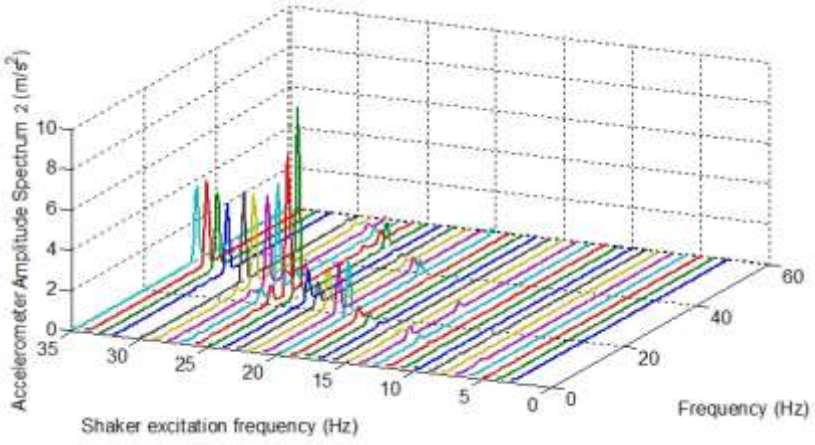

Fig. 13: Fourier amplitude spectrum for the acceleration of the blade read by accelerometer 2

Figure 13 shows that the mode shape corresponding to a frequency around f=25Hz, shown by the green curve, can create considerable acceleration helpful for shaking off the ice. Other accelerometers also show high values of acceleration at this frequency, which is consistent with the modelling results. Figure 14 presents the maximum amplitudes of accelerations measured at each accelerometer position as a function of frequency excitation. As seen in the plot, the two mode shapes with the resonance frequencies of 21 Hz and 25 Hz generate the highest acceleration making them suitable for ice removal.

The main objective of this work (operational modal analysis), i.e. identification of the mode shapes, especially the third flexural bending modes, was achieved as the result compares satisfactorily with the modelling results.

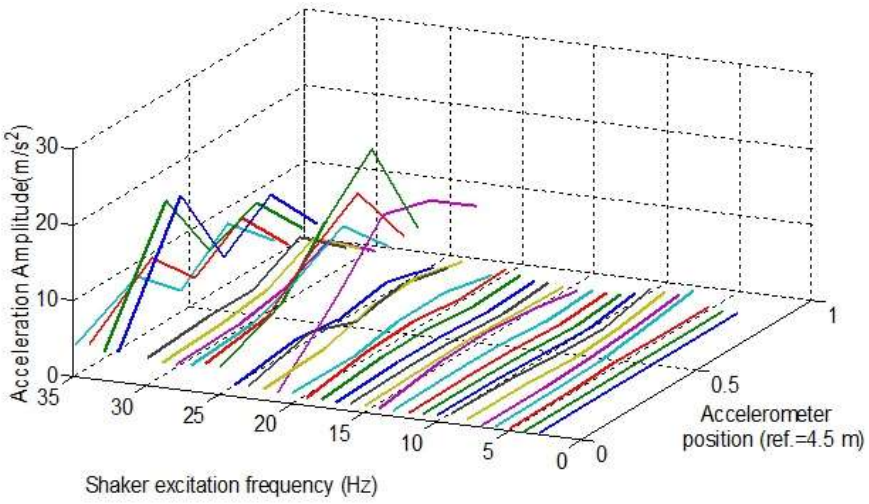

Fig. 14: Maximum acceleration obtained at each acceleration position over the excitation frequency spectra.

3.1.2. UGW tests

For the laboratory trials, UGWs were propagated in a range of steel, aluminum and glass reinforced plastic plates, 0.5mm – 2mm and small enough to place inside a freezer, with UGW actuators clamped to the plate (Fig. 15). An Agilent Technologies digital oscilloscope type MSO-X 302A was used to generate a constant sine wave voltage, up to a maximum of 5V peak-to-peak, over a range of frequencies from the Hz into MHz ranges. 5V peak to peak was found to be adequate for most of the experimental work here, though a 10V output Instek sine wave generator type 8216A was also used to give higher voltages. The sine wave generator was connected to an EIN RF power amplifier type 240L to generate the voltage amplitudes necessary to drive the shear actuators. These voltages ranged from 50V to 200V peak-to-peak.

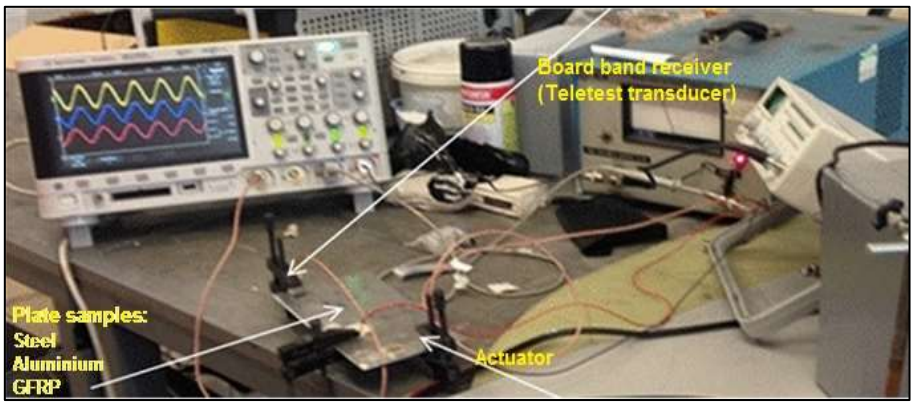

Fig. 15: Typical experimental set-up

To create ice on the surfaces of the plate, plates were placed inside a domestic freezer (Fig. 16*a*).

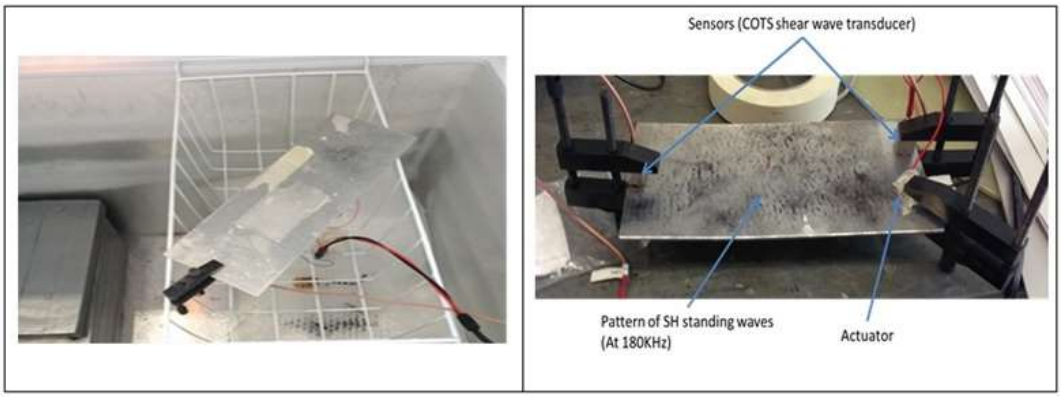

Fig. 16: The test plate in experiment, a) Ice patches created in freezer; b) Standing SH wave patterns in iron oxide powder

Validation of the numerical models of ice debonding experimentally from the substrate with Shear-Horizontal (SH) guided ultrasonic waves proved to be impossible. The time it took to remove the ice was a determining variable and this varied according to the thickness of the ice, its distance from the actuator, the nature of the substrate and even the ambient temperature. Moreover, the actuators generate heat and it was not always possible to determine whether or not this was causing the ice to melt, rather than SH-waves causing the ice to substrate bond to break. A real-time metric was needed.

One discovery was that fine black iron oxide particles, used in magnetic particle inspection, could visualize SH standing waves in the plates. This was a very useful phenomenon, because the patterns would only appear when resonances occurred in the plate, and the distances between the nodes and anti-nodes could be measured to provide measurements of wavelength. The particles move in response to the shear stresses on the plate surfaces, which, in the presence of standing waves, give rise to patterns in the powder distribution (Fig. 16b). To apply the powder evenly, a dry powder puffer bulb was used.

Another metric was to measure the displacement at the surface with a shear wave sensor. Transducers from the commercially available Teletest Long Range Ultrasonic Testing (LRUT) system were used for this purpose. These have shear wave elements that are highly damped, in order to give short pulses of ultrasound with minimum ‘ringing’ that are needed in pulse-echo ultrasonics. The damping gives the transducers very broad band receiver response. The Teletest transducer was connected to the same oscilloscope as the actuators so that both the transmitted and received sine waves could be observed and phase shifts and amplitude changes could be observed in response to changes in frequency.

The Teletest shear transducer is designed for pulse-echo ultrasonic testing. It is therefore heavily damped and of low power output. A range of alternative high-power shear wave actuators including Lead Zirconium Titanate piezoelectric (PZT) and resonating Macro-Fibre-Composites (MFCs) were investigated (Fig. 17).

MFCs were first investigated as these give relatively large displacements (>10microns) with moderate applied voltages (<200 V). However, the shear actuation is complicated by the bipolar nature of the motion, where the ends of the MFC element move in and out in unison and the middle element is stationary. This in effect creates two SH waves.

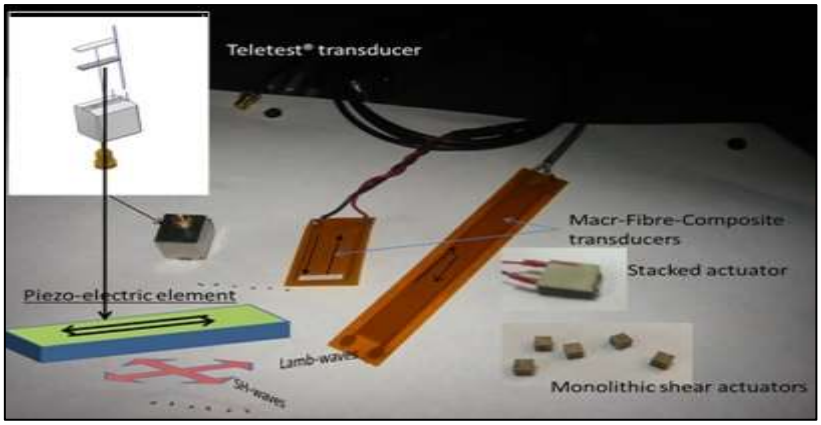

Fig. 17: Actuators used in the experiments

A range of 6mm x 6mm and 10mm x 10mm PZT actuators, 1.7mm and 3.4mm thick with either single (X or Y direction) or dual (X and Y direction) motion were acquired. It was found that the thickness of the shear actuator determined the amount of displacement with each stroke of the applied voltage - the thicker the element, the greater the voltage needed to power it. To increase the magnitude of the actuator displacement, it is possible to stack two or more elements together separated by electrodes. The experiments conducted here used two-element stacked actuators.

The actuator was placed close to one end of the plate, and the shear wave sensor at the other. For the de-icing experiments, after the ice had formed, the plate was held vertical in the ice box or freezer. For the visualization experiments, the plate surface, which had been carefully dried, was held horizontal.

The initial experiments with the available PZT shear actuators attempting to break the ice to substrate bond did show some debonding of the ice from the substrate, but this could have been a thermal effect rather than a mechanical one. A new study of standing SH-waves in the plates using the iron oxide powder as the detecting medium and the LRUT shear transducer as the SH-wave sensor was performed. A parametric study was set up to find the influencing factors on the amplitude of standing SH waves (Table 3). In this study, the temperature of both ambient and freezer were changed to see their effects on the performance of the waves. Likewise actuators of different orientations for propagating waves, different positions and different resonating pressure were examined. Also the orientations of receivers were being varied to ensure the reception of maximum wave amplitude.

Table 3: Matrix of parameters

Temperature		Actuator											Receiver	
Ambient	Freezer	Orientation		Position						Pressure (per unit area)			Orientation	
20C	-10C	X	Y	15.5/5	15.5/6	15.5/7.5	25/5	27/5	29/5	0.3 N	0.4 N	0.5 N	X	Y

For each experiment a frequency sweep was conducted, starting at just within the audible frequency range (15 kHz) and ending at about 350 kHz, according to whether or not a voltage

could be detected at the sensor. A typical data record is shown in Fig. 18, the peaks in the voltages at the sensors occurring at the plate SH-wave resonances.

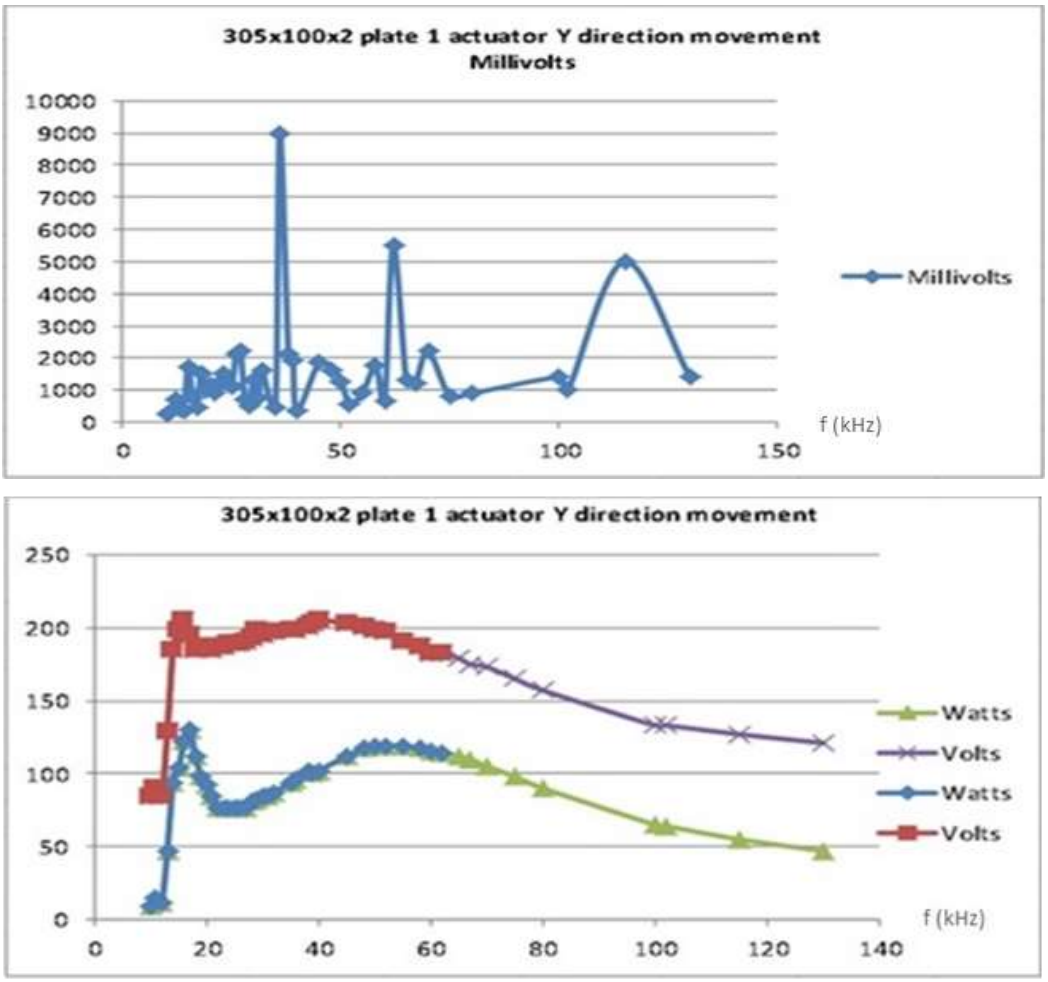

Fig. 18: Example experiment data set

The parametric study showed that the dominant influence on plate resonance was plate width.

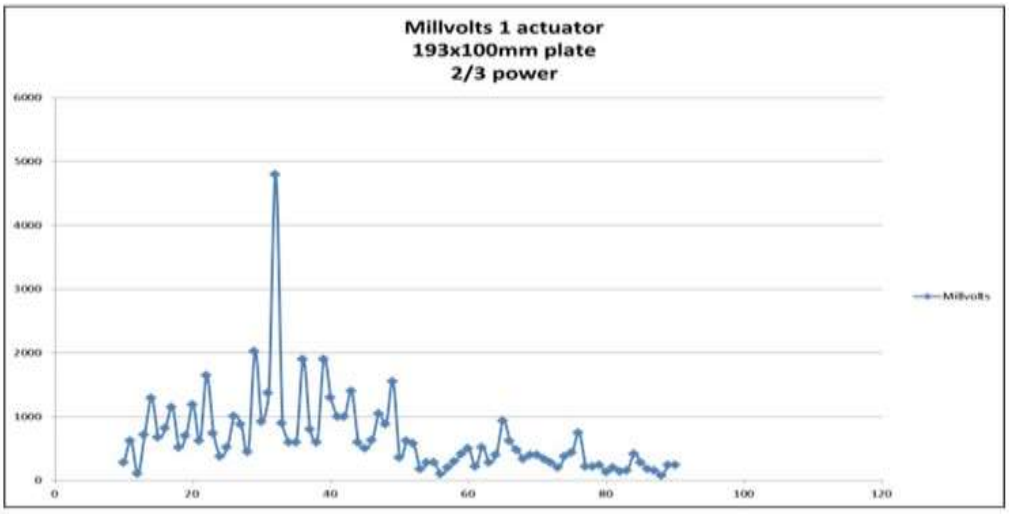

Fig. 19: Peak resonance in 100mm wide Al plate

With the actuator placed in the middle of the plate, the first resonance would occur when the plate width was equal to ½ wavelength of the S0 wave (Fig. 19). This is due to the shear wave actuator propagating a Lamb wave orthogonal to the SH wave (Fig. 20). The Lamb wave component is shown in the upper part of the figure, the SH wave component in the lower part. The graphs show the respective Dispersion curves, from which values for wavelength of Lamb waves and SH-waves at different frequencies in a 2mm thick Al strip have been derived. Lamb waves are made more complicated than SH waves by the presence of symmetric and anti-symmetric motions.

The parametric study also concluded that shear horizontal waves (SH waves) are attenuated too strongly in GFRP to be used for de-icing the leading edge of a wind turbine blade. Therefore, as an innovative solution, it was proposed to use an aluminium strip mounted on leading edge of the blade, to which the SH-wave actuators were attached. A schematic of the shield and its dimension details along with an ultrasonic actuator array placed along its centre-line is shown in Fig. 21.

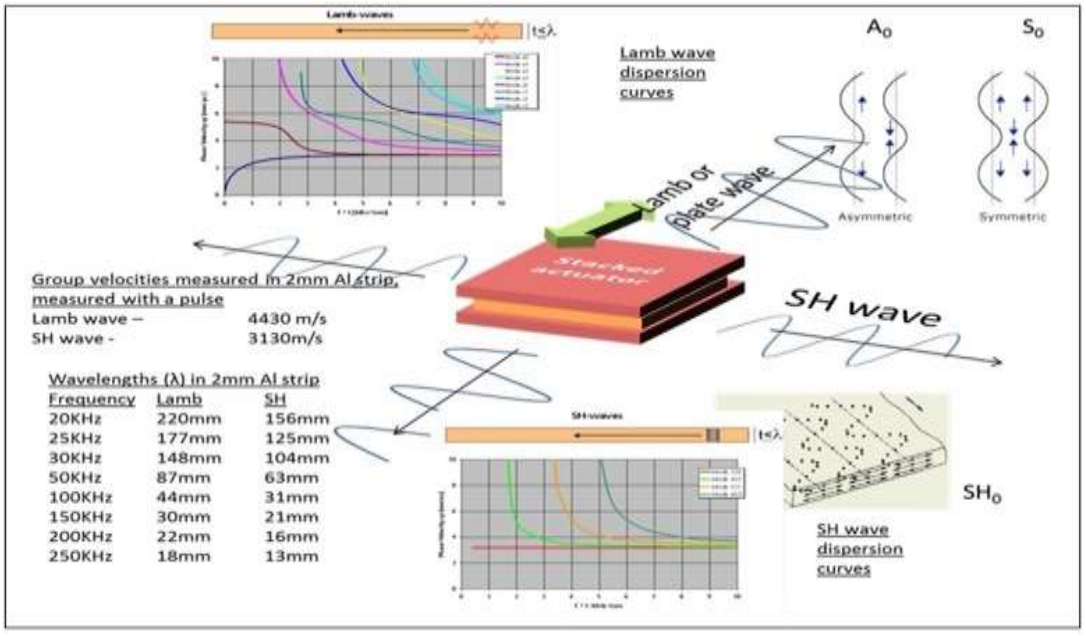

Fig. 20: Orthogonal SH and Lamb waves from actuator

The power required for protecting the Al strip shown in Fig. 21 was almost 400 W consumed by the 4-transducer array to be used for a single blade. This means that the total power consumption for a three-blade wind turbine would be 1200 W, 1.6% of the turbine's nominal power output (as the modelled blade is pertinent to a 75-kW wind turbine). This amount of power is a considerable reduction compared to the power consumed by thermal de-icing techniques which usually reaches up to 15% [2].

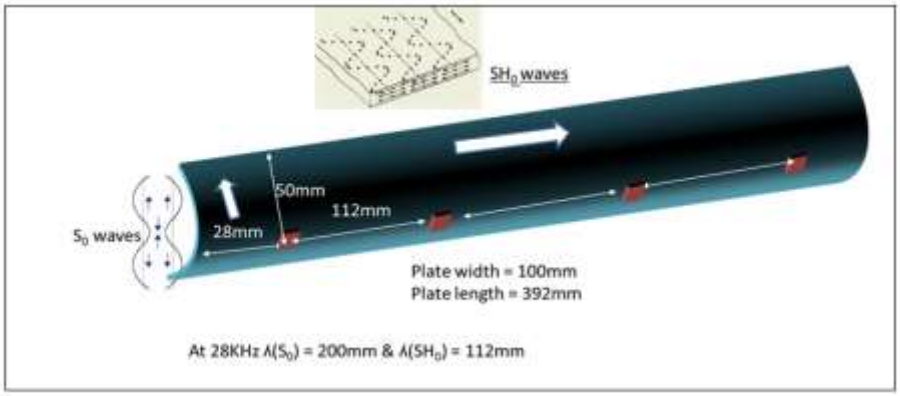

Fig. 21: Design for de-icing shield along leading edge of turbine blade

3.2. Wind tunnel testing

Once reliability and performance of both the UGW and LFV techniques were verified in the laboratory experiments, the approach was tested in a climatic chamber with interior dimensions of 3300mm x 3555mm x 7000mm. The tunnel air temperature could reach down to -40^{o}C with possibility to apply different relative humidity ranging from 5% to 95%. The chamber had fully enclosed support building with a circuit type of vertical return. It was provided by two airflow nozzles and a cooling system of 765kW capacity supplied by twin rotary-screw compressors and heat exchangers.

The procedure in the icing tunnel was application of the integrated setup to investigate the synergistic effects of this approach. The mock-up wind turbine blade provided by the shaker setup and ultrasonic transducer array was then subjected to ice formation in the wind tunnel under freezing conditions. The temperature during the experiment was kept in a constant domain between -18 ^{o}C to -21 ^{o}C. Also, the relative humidity was always near to saturation ranging from about 80% to 95%. Forming the ice was carried out using a special water sprayer/gun driven by high pressure air. Since the type of ice built up depends on a few factors such as water droplet size, chamber humidity, temperature and airflow velocity, various types of ice were formed under certain conditions. Fig. 22 shows the three types of ice created on the blade during trials in the wind tunnel.

(*a*) (b) (c)

Fig. 22: Different types of ice formed in icing wind tunnel; *a*) hard rime ice, b) clear glaze ice, c) soft frost (snow-looking ice)

The performance of the approach to tackle ice accumulation depends on the ice type. Since humidity and temperature in the chamber were changing in a narrow domain, the type of formed ice was highly dependent on the way water sprayed on the blade surface. In fact, it is important that how far the water gun is operated from the target surface. This factor determines the size and instant temperature of water droplets as well as the speed of their impingement to the blade. The major ice shape built up was *hard rime* ice which is a milky-looking ice with a comb-like appearance that usually forms with high velocities. This type, shown in Fig. 22a, is a very hard ice found in nature. In the wind tunnel, this type appeared to accrete mostly when water sprayed on the blade surface from a distance of approximately 0.6m to 0.7m. The height of the teeth of a rime ice layer, on average reached up to about 10mm within roughly one hour constant spraying.

The closer the water gun is to target surface, the higher is speed of impingement of water droplets. On the other hand, when water was sprayed from a further distance, the droplets became more scattered and finer with more chance for heat transfer with ambient. Once the water spray jet was approaching to the blade, the ice became clearer and smoother so that in a distance less than 20cm away, a transparent and quite homogenous ice coating so called clear glaze ice (shown in Fig. 22b) was built up. It took around 60 minutes to form a 5mm thick layer glaze ice. This type normally forms due to the impact of water droplets at temperatures near freezing [13].

In addition to the high hardness of rime ice, it is mentionable that the characteristics assumed for the theoretical studies and modelling procedures were not correlated to this type but rather to the properties of glaze ice. For these reasons, although the developed strategy was able to cause some cracks of up to almost 10 cm long in the layers of rime ice, it was unable to achieve complete ice removal. On the contrary, as shown in Fig. 23, the transducer array with the complementary effects of shaker setup could cope with removal of the glaze ice. This removal occurred first for about a 20-cm long patch of the 5-mm thick ice layer (around half of the Al bent plate representing the leading edge) almost instantly after the ice protection system was switched on. The other half of ice patch was shed off within two seconds after start-up. Except two very narrow strips hooked on the edges of the bent plate, there were no even tiny spots remaining on the entire leading edge. This observation was verified through two more attempts under same conditions while similar results were achieved each time.

Fig. 23: A de-bonded layer of glaze ice formed on the Al strip mounted on the blade leading edge

In terms of the third type of ice i.e. snow-like, soft frost, the integrated setup could cope with it as shown in Fig. 22c. Although there were a few small ice patches of about 8mm thickness remaining on the lower parts of the blade, but the most crucial area i.e. the top strip of the leading edge became entirely ice-free within 2-sec of the system operation. This soft form appeared when the water spray was used more than a meter away from the blade surface. Under this condition, the airflow was much slower and the water droplets became even finer compared to the other two forms. In such a long range that droplets hit the surface, they have more chance for heat transfer with ambient and therefore becoming cooler. Since the bond of this type is not very firm and its density is very low compared to the other two types, the performance of the shaker setup was understandably more effective than the UGW transducer array.

It should also be noted that, in the wind tunnel, it was not feasible to take into account the effects of centrifugal force arising from rotation of the wind turbine propeller. While the wind hitting the blade was simulated in the chamber, this force acting on the ice layers could obviously be helpful in stripping off the ice. For this reason, it can be stated that the approach performance could have been even more effective in presence of centrifugal forces. According to some preliminary simulation, this force is even stronger than the force caused by LFV but since it applies as in-plane direction, it is not as effective as the normal-to-plane LFV forces. Therefore, the approach is recommended to be tested under real conditions as field trials where the turbine propeller spins.

4. Concluding remarks

In this study, a new approach to protect wind turbine blades against icing problems was presented. The strategy is based on the superimposition of ultrasonic guided waves (UGW) with low frequency vibrations (LFV) in such a way that the UGW shortcomings are compensated by LFV. In fact, UGW has already been applied to ice protection systems but has been never combined with any other type of vibration to improve its efficiency. In this work, while the UGW technique was adapted for an anti/de-icing system for a mock-up wind turbine blade, its functionality with the supplementary effects of LFV was enhanced further. In fact, as the UGW approach takes care of the main action in generating shear stresses to de-bond the ice layer accreted on the blade, the LFV shaker setup applies excessive stress through high accelerations within a short period of operation to complement UGW's performance and shed the ice.

The initial challenge was to characterise the optimum parameters of the UGW technique through FEM modelling and post-processing analysis: best wave mode, excitation frequency, excitation direction, number and geometry of transducer array to propagate the ultrasonic waves using a minimal power were determined. At the same time, an FEM model of the full-scale blade was developed for modal and harmonic analyses from which the optimum characteristics of the shaker setup were evaluated. Then, laboratory trials to validate modelling results obtained for LFV performance were implemented on the blade. The trials included a strain gauge setup, to measure displacements, and operational modal analysis, through an accelerometer setup, to characterise mode shapes. The data obtained by

experimental post-processed data and modelling results were in reasonable agreement. Regarding the UGW experimental tests, as expected according to the modelling results, the waves were strongly attenuated in the composite test pieces. Hence, as a novel solution, the tests were carried out for an aluminium strip to be bent and mounted on the leading edge of the blade as a shield in order to conduct the waves efficiently for ice removal. The required power turned out to be very low compared to thermal ice protection systems making it an efficient technique.

As the final phase, the blade was tested in an icing wind tunnel using the final setup integrating LFV and UGW strategies. Different forms of ice were developed on the blade in a climatic chamber. Since the technique development has been based on considering glaze ice properties, the approach could cope with removing the clear glaze ice and soft frost when both UGW and LFV are applied in a synergistic way as planned. Although the approach was not entirely successful in the case of hard rime ice, there were some promising indications that the approach could work even for hard rime ice, if the properties of this ice form were considered in developing the technique.

Acknowledgements

This paper is a technical summary extracted from a project called DeICE-UT. The DeICE-UT project is co-founded by the European Commission through the Seventh Framework Programme (FP7/2007-2013) managed by REA-Research Executive Agency through the funding scheme “Research for the Benefit of SMEs” under Grant Agreement No.605138. DeICE-UT is collaboration between the following organisations: TWI, Brunel University London, ZUT, BS Rotor, DTK Electronics, Selftech, Smart Material, Floteks and Tureb.

References

[1] Rindeskär E., Modelling of icing for wind farms in cold climate, Examensarbete vid Institutionen för Geovetenskaper, ISSN 1650-6553 Nr 20, 2010

[2] Laakso T., Peltola E., Review on blade heating technology and future prospects, *Proceedings of BOREAS VII International Conference*, March 2005, Saariselka, Finland, pp.12.

[3] Sørensen J.D., Sørensen J.N., Wind energy systems: optimising design and construction for safe and reliable operation, Woodhead Publishing Ltd., UK, 2011.

[4] Kimura S., Sato T., Kosugi K., The effects of anti-icing paint on the adhesion force of ice accretion on a wind turbine blade, *Proceedings of BOREAS VI International Conference*, April 2004, Finish Meteorological Institute, Pyhatunturi, Finland, pp. 9.

[5] Gao H.D., Rose J.L., Ice Detection and Classification on an Aircraft Wing with Ultrasonic Shear Horizontal Guided Waves, *Ultrasonics, Ferroelectrics and Frequency Control*, Vol. 56, Issue: 2, 334-344, 2009.

524 [6] Palacios J.L., Design fabrication and testing of an ultrasonic de-icing system for
525 helicopter rotor blades, *PhD Thesis*, the Pennsylvania State University, Engineering
526 Science and Mechanics, 2008.

527 [7] Overmeyer A., Palacios J., and Smith E., Ultrasonic De-Icing Bondline Design and Rotor
528 Ice Testing, AIAA Journal, Vol. 51, No. 12 (2013), pp. 2965-2976. doi:10.2514/1.J052601

529 [8] Zhu Y.,Structural tailoring and actuation studies for low power ultrasonic de-icing of
530 aluminium and composite plates**,** *PhD Thesis*, the Pennsylvania State University,
531 Engineering Science and Mechanics, 2010.

532 [9] Coffman H.J., Helicopter Rotor Icing Protection Methods, Bell Helicopter Textron Inc.,
533 Fort Worth Texas, *Journal of the American Helicopter Society*, 1987.

534 [10] Stallabrass J.R., Price R. D., On the Adhesion of Ice to Various Materials, *Canadian*
535 *Aeronautics and Space*, 1963, 199-203.

536 [11] Zhao, F. M., Takeda, N., Effect of Interfacial Adhesion and Statistical Fiber Strength on
537 Tensile Strength of Unidirectional Glass Fiber/Epoxy Composites, *Composite*, Part A, pp.
538 1203- 1214, 2000.

539 [12] Sutherland H.J., On the Fatigue Analysis of Wind Turbines, *Sandia National Laboratories*,
540 Albuquerque, New Mexico 87185-0708, June 1999.

541 [13] Hansman, R.J., Yamaguchi, K., Berkowitz, B., and Potapczuk, M., Modeling of surface
542 roughness effects on glaze ice accretion", *Journal of Thermophysics and Heat Transfer*,
543 Vol. 5, No. 1 (1991), pp. 54-60. doi: 10.2514/3.226

544